Inorganic Chemistry
Article

Inorg. Chem. **2010**, *49*, 9683–9688 **9683**
DOI: 10.1021/ic101431g

Synthesis, Crystal Structure, and Magnetic Properties of the Copper Selenite Chloride $Cu_5(SeO_3)_4Cl_2$

Dong Zhang,[†,‡] Helmuth Berger,[§] Reinhard K. Kremer,[⊥] Dirk Wulferding,[¶] Peter Lemmens,[¶] and Mats Johnsson*[,‡]

[†]*College of Physics/State Key Laboratory of Superhard Materials, Jilin University, 130012, Changchun, People's Republic of China,* [‡]*Division of Inorganic and Structural Chemistry, Department of Materials and Environmental Chemistry, Stockholm University, S-106 91 Stockholm, Sweden,* [§]*Institute of Condensed Matter Physics, Ecole Polytechnique Fédérale de Lausanne (EPFL), CH-1015, Lausanne, Switzerland,* [⊥]*Max Planck Institute for Solid State Research, Heisenbergstrasse 1, D-70569 Stuttgart, Germany, and* [¶]*Institute for Physics of Condensed Matter, TU Braunschweig, D-38106 Braunschweig, Germany*

Received July 18, 2010

A new copper selenite chloride $Cu_5(SeO_3)_4Cl_2$ has been prepared by chemical vapor transport reactions. Its crystal structure was determined by single-crystal X-ray diffraction. The title compound crystallizes in the monoclinic space group $P2_1/c$ with the unit cell parameters $a = 10.9104(8)$ Å, $b = 8.3134(6)$ Å, $c = 7.5490(6)$ Å, $\beta = 90.715(6)°$, $Z = 2$, and $R_1 = 0.0383$. Bond valence sum calculations indicate that the cations have the oxidation state Cu(II) and Se(IV), respectively. Three crystallographic different copper atoms, having different coordination polyhedra, $[CuO_5]$, $[CuO_6]$, and $[CuO_3Cl_2]$, are connected by corner and edge sharing to form a framework that can be described as metal−oxygen slabs connected by Cl atoms via edge sharing $[CuO_3Cl_2]$ polyhedra. The two crystallographic different selenium atoms both have $[SeO_3E]$ coordination, where E is the $4s^2$ lone pair on Se(IV); they are isolated from each other and do bond to the Cu-coordination polyhedra only. The magnetic properties of the Cu^{2+} ions with effective spin $S = 1/2$ moments are dominated by antiferromagnetic interactions. For temperatures $T < T_c \sim 45$ K, Néel magnetic ordering is observed with small ferromagnetic canted moments. We attribute these to antisymmetric Dzyaloshinskii−Moriya (DM) spin exchange which is allowed by the low symmetry spin exchange paths along the distorted transition metal oxyhalide coordinations.

Introduction

The crystal chemistry of oxohalides comprising a p-element having a stereochemically active lone pair (such as Sb^{3+}, Se^{4+}, Te^{4+}, etc.) and a late transition metal has proven to be rich, and a number of such compounds have previously been described, e.g., $CuSb_2O_3Br$,[1] $Ni_5(SeO_3)_4X_2$ (X = Cl, Br),[3,4] and $Fe_3Te_3O_{10}Cl$.[5] The presence of a stereochemically active lone pair will allow for asymmetric or one-sided coordination around the lone-pair cation. It does not participate in bonding and occupies a volume similar to that of an oxygen atom[6] and is, thus, large enough to open up the crystal structure significantly. The role of lone-pair distortions in structural chemistry has been addressed by several workers over the past six decades.[7−14]

Most commonly, the lone-pair cations only coordinate oxygen while late transition metal cations bond to both oxygen and halide ions in oxohalide compounds. This is due to the stronger Lewis acidity of the lone pair cation compared to the late transition metal cation. A result is that both the lone pairs and the halide ions act as "chemical scissors" opening up the crystal structure and reducing its dimensionality. Further, this is a reason why many such compounds exhibit a layered crystal structure where the lone pairs and the halides protrude from the layers and only weak van der Waal bonds connect the layers as, e.g., with $Ni_5(TeO_3)_4Cl_2$[15] or porous structures

*To whom correspondence should be addressed. Fax: +46-8-15 21 87. Tel: +46-8-16 21 69. E-mail: matsj@inorg.su.se.

(1) Mayerová, Z.; Johnsson, M.; Lidin, S. *J. Solid State Chem.* **2005**, *178*, 3471–3475.
(3) Shen, Y.-L.; Mao, J.-G.; Jiang, H.-L. *J. Solid State Chem.* **2005**, *178*, 2942–2946.
(4) Jiang, H.-L.; Mao, J.-G. *Inorg. Chem.* **2006**, *45*, 7593–7599.
(5) Zhang, D.; Johnsson, M.; Berger, H.; Kremer, R. K.; Wulferding, D.; Lemmens, P. *Inorg. Chem.* **2009**, *48*, 6599–6603.
(6) Galy, J.; Meunier, G.; Andersson, S.; Åström, A. *J. Solid State Chem.* **1975**, *13*, 142–159.
(7) Sidgwick, N. V.; Powell, H. M. *Proc. R. Soc.* (*London*) **1940**, *A176*, 153–180.
(8) Gillespie, R. J.; Nyholm, R. S. *Quart. Rev.* (*London*) **1957**, *11*, 339–380.
(9) Orgel, L. E. *J. Chem. Soc.* **1959**, *4*, 3815–3819.
(10) Ok, K. M.; Halasyamani, P. S. *Inorg. Chem.* **2002**, *41*, 3805–3807.
(11) Ok, K. M.; Halasyamani, P. S. *Angew. Chem., Int. Ed.* **2004**, *43*, 5489–5491.
(12) Seshadri, R.; Hill, N. A. *Chem. Mater.* **2001**, *13*, 2892–2899.
(13) Stoltzfus, W.; Woodward, P. M.; Seshadri, R.; Klepeis, J.-H.; Bursten, B. *Inorg. Chem.* **2007**, *46*, 3839–3850.
(14) Waghmare, U. V.; Spaldin, N. A.; Kandpal, H. C.; Seshadri, R. *Phys. Rev. B* **2003**, *67*, 125111/1–1255111/10.
(15) Johnsson, M.; Törnroos, K. W.; Lemmens, P.; Millet, P. *Chem. Mater.* **2003**, *15*, 68–73.

Published on Web 09/21/2010

Table 1. Crystal Data and Structure Refinement Parameters for $Cu_5(SeO_3)_4Cl_2$

empirical formula	$Cu_5(SeO_3)_4Cl_2$
formula weight	896.44
temperature (K)	293(2)
wavelength (Å)	0.71073
crystal system	monoclinic
space group	$P2_1/c$
a (Å)	10.9104(8)
b (Å)	8.3134(6)
c (Å)	7.5490(5)
β (°)	90.715(6)
volume (Å ^{3})	684.66(8)
Z	2
density$_{calc.}$ (g cm^{-3})	4.348
absorption coefficient (mm^{-1})	18.721
F (000)	822
crystal size	0.2530 × 0.1144 × 0.0374
θ range for data collection (°)	4.11−26.35
index ranges	$-13 \le h \le 13$, $-10 \le k \le 8$, $-9 \le 1 \le = 9$
reflections collected	4423
independent reflections	1367 [R(int) = 0.0826]
data/restraints/parameters	1367/0/107
refinement method	full-matrix least-squares on F^2
goodness-of-fit on F^2	1.009
final R indices [$I > 2\sigma$(I)][a]	R_1 = 0.0383
	wR_2 = 0.0904
R indices (all data)	R_1 = 0.0427
	wR_2 = 0.0924
largest diff. peak and hole (e Å^{-3})	1.697 and −1.044

[a] $R_1 = \sum\|F_o| - |F_c\|/\sum|F_o|$; $wR_2 = \{\sum[w(F_o^2 - F_c^2)^2]/\sum[w(F_o^2)^2]\}^{1/2}$.

where the lone pairs instead occupy space in the pores that also face the halide ions, e.g., $Co_7(TeO_3)_4Br_6$.[16] Several oxohalide compounds have unusual magnetic properties that result from spin frustration due to the topology of the compounds: $FeTe_2O_5Cl$,[17,18] $Cu_4Te_5O_{12}Cl_4$,[19] and $Cu_2Te_2O_5Cl_2$.[20]

In this work, we report the synthesis and magnetic properties of $Cu_5(SeO_3)_4Cl_2$ which constitute a new oxohalide compound in the system $Cu^{2+}-Se^{4+}-O-Cl$. There are previously many oxohalides described in the same system and surprisingly many of them are minerals from Kamchatka and some of them are synthetic compounds: α-$Cu_5(SeO_3)_2O_2Cl_2$,[2,21] β-$Cu_5(SeO_3)_2O_2Cl_2$,[22] α-$Cu_9Se_4O_{14}Cl_6$,[23] β-$Cu_9Se_4O_{14}Cl_6$,[24] α-$Cu_3(SeO_3)_2Cl_2$,[25] β-$Cu_3(SeO_3)_2Cl_2$,[26] and the mixed Cu^+/Cu^{2+} compound $Cu_5(SeO_3)OCl_5$.[27]

Table 2. Atomic Coordinates (×10^4) and Equivalent Isotropic Displacement Parameters (Å^2 × 10^3) for $Cu_5(SeO_3)_4Cl_2$

atom	x	y	z	U (eq)[a]
Se(1)	8206(1)	9036(1)	34(1)	11(1)
Se(2)	3790(1)	6871(1)	1663(1)	10(1)
Cu(1)	6327(1)	6280(1)	1577(1)	13(1)
Cu(2)	5000	5000	5000	11(1)
Cu(3)	1412(1)	5036(1)	788(1)	14(1)
Cl(1)	−376(2)	3801(2)	1586(2)	19(1)
O(1)	7873(5)	10088(6)	1871(6)	23(1)
O(2)	7803(4)	7109(5)	604(6)	17(1)
O(3)	6981(4)	5337(5)	3791(5)	15(1)
O(4)	4765(4)	5363(5)	2401(5)	13(1)
O(5)	4986(4)	7664(5)	429(5)	13(1)
O(6)	2994(4)	5941(5)	25(5)	14(1)

[a] Note: U(eq) is defined as one third of the trace of the orthogonalized U_{ij} tensor.

Experimental Section

Single crystals of $Cu_4Se_5O_{12}Cl_2$ have been grown by a standard chemical vapor phase method. Mixtures of high purity CuO (Alfa-Aesar, 99.995%), $CuCl_2$ (Alfa-Aesar, 99.995%), and SeO_2 (Alfa-Aesar, 99.999%) powder in molar ratio 3:2:5 were sealed in quartz tubes with electronic grade HCl as transport gas for the crystal growth. The quartz ampules employed were 250 mm in length with a diameter of 34 mm. The ampules were placed horizontally into a tubular two-zone furnace and heated very slowly with a rate of 25 °C/h to 450 °C. For the growth of single crystals, the optimum temperatures at the source and deposition zones have been established as 450 and 300 °C, respectively. After 6 weeks, several green platelet shaped crystals of $Cu_4Se_5O_{12}Cl_2$ and $CuSe_2O_5$ were observed (roughly 10% of the bulk powder). Thin crystals of the title compound of up to 5 mm in length were obtained. The elemental composition of all heavy elements in the synthesis product was confirmed using energy-dispersive spectrometry (EDS) in a scanning electron microscope (SEM, JSM-7000F).

Single crystal X-ray data were collected at 293 K on an Oxford Diffraction Xcalibur 3 diffractometer system using graphite monochromatized Mo Kα radiation, λ = 0.71073 Å. Integration of the reflection intensities and absorption correction were performed using the software provided by the diffractometer manufacturer. The structure was solved by Direct Methods, using the SHELXTL crystallographic software package.[28] The selenium and copper atoms were first located, whereas the chlorine and oxygen atoms were found in the difference Fourier maps. All atoms were refined with anisotropic temperature factors. Details of the final refinement are compiled in Table 1. Atomic coordinates and equivalent isotropic displacement parameters are reported in Table 2. Selected bond lengths and angles are listed in Table 3. The structural drawings are made with the program DIAMOND.[29]

A number of small single crystals were collected, crushed, and checked with a Panalytical X'Pert PRO powder diffractometer. The diffraction peaks on experimental and simulated XRD patterns corresponded well in Bragg angle and intensity, indicating the purity of the as-synthesized samples. The material used for magnetic and heat capacity measurements was selected from the same batch of small single crystals.

Magnetic susceptibilities of a crystal (∼1 mg, field aligned along the crystal plate that is the (010) plane) were measured as a function of magnetic field and temperature with a MPMS SQUID magnetometer (Quantum Design, San Diego, CA) The heat capacities were determined in a PPMS system

(16) Becker, R.; Johnsson, M.; Berger, H.; Prester, M.; Zivkovic, I.; Drobac, D.; Miljak, M.; Herak, M. *Solid State Sci.* **2006**, *8*, 836–842.
(17) Becker, R.; Johnsson, M.; Kremer, R. K.; Klauss, H. H.; Lemmens, P. *J. Am. Chem. Soc.* **2006**, *128*, 15469–15475.
(18) Pregelj, M.; Zaharko, O.; Zorko, A.; Kutnjak, Z.; Jeglič, P.; Brown, P. J.; Jagodič, M.; Jagličić, Z.; Berger, H.; Arčon, D. *Phys. Rev. Lett.* **2009**, *103*, 147202/1–147202/4.
(19) Takagi, R.; Johnsson, M.; Gnezdilov, V.; Kremer, R. K.; Brenig, W.; Lemmens, P. *Phys. Rev.* **2006**, *B74*, 014413/1–014413/7.
(20) Johnsson, M.; Törnroos, K. W.; Mila, F.; Millet, P. *Chem. Mater.* **2000**, *12*, 2853–2857.
(21) Krivovichev, S. V.; Shuvalov, R. R.; Semenova, T. F.; Filatov, S. K. *Z. Kristallogr.* **1999**, *214*, 135–138.
(22) Krivovichev, S. V.; Filatov, S. K.; Burns, P. C.; Vergasova, L. P. *Can. Mineral.* **2007**, *45*, 929–934.
(23) Krivovichev, S. V.; Filatov, S. K.; Semenova, T. F.; Rozhdestvenskaya, I. V. *Z. Kristallogr.* **1998**, *213*, 645–649.
(24) Bastide, B.; Millet, P.; Johnsson, M.; Galy, J. *Mater. Res. Bull.* **2000**, *35*, 847–855.
(25) Millet, P.; Bastide, B.; Johnsson, M. *Solid State Commun.* **2000**, *113*, 719–723.
(26) Becker, R.; Berger, H.; Johnsson, M. *Acta Crystallogr., Sect. C* **2007**, *63*, i4–i6.
(27) Krivovichev, S. V.; Filatov, S. K.; Armbruster, T.; Pankratova, O. Yu. *Dokl. Akad. Nauk* **2004**, *399*, 356–358.
(28) Sheldrick, G. M. *Acta Crystallogr.* **2008**, *A64*, 112–122.
(29) Bergerhoff, G. *Diamond*; Computer program from Crystal Impact GbR: Bonn, Germany, 1996.

Table 3. Selected Bond Lengths (Å) and Angles (°) for $Cu_5(SeO_3)_4Cl_2$[a]

Se(1)−O(1)	1.682(4)	Se(2)−O(6)	1.690(4)
Se(1)−O(3)#1	1.705(4)	Se(2)−O(4)	1.732(4)
Se(1)−O(2)	1.717(4)	Se(2)−O(5)	1.743(4)
Cu(1)−O(2)	1.907(4)	Cu(3)−O(1)#4	1.923(5)
Cu(1)−O(3)	1.972(4)	Cu(3)−O(6)	1.975(4)
Cu(1)−O(4)	1.974(4)	Cu(3)−O(2)#2	2.245(4)
Cu(1)−O(5)	2.045(4)	Cu(3)−Cl(1)	2.2917(18)
Cu(1)−O(6)#2	2.333(4)	Cu(3)−Cl(1)#6	2.3188(17)
Cu(2)−O(5)#3	1.969(4)	Cu(2)−O(4)#5	1.998(4)
Cu(2)−O(5)#4	1.969(4)	Cu(2)−O(3)#5	2.374(5)
Cu(2)−O(4)	1.998(4)	Cu(2)−O(3)	2.374(5)
O(1)−Se(1)−O(3)#1	96.9(2)	O(6)−Se(2)−O(4)	102.3(2)
O(1)−Se(1)−O(2)	102.7(2)	O(6)−Se(2)−O(5)	99.4(2)
O(3)#1-Se(1)−O(2)	102.8(2)	O(4)−Se(2)−O(5)	89.1(2)
O(2)−Cu(1)−O(3)	99.86(19)	O(1)#4-Cu(3)−O(6)	85.06(19)
O(2)−Cu(1)−O(4)	175.65(19)	O(1)#4-Cu(3)−O(2)#2	107.20(19)
O(3)−Cu(1)−O(4)	83.34(18)	O(6)−Cu(3)−O(2)#2	80.01(17)
O(2)−Cu(1)−O(5)	103.70(18)	O(1)#4-Cu(3)−Cl(1)	96.03(15)
O(3)−Cu(1)−O(5)	146.33(17)	O(6)−Cu(3)−Cl(1)	175.61(13)
O(4)−Cu(1)−O(5)	74.65(16)	O(2)#2-Cu(3)−Cl(1)	95.61(12)
O(2)−Cu(1)−O(6)#2	79.12(17)	O(1)#4-Cu(3)−Cl(1)#6	152.77(15)
O(3)−Cu(1)−O(6)#2	90.60(16)	O(6)−Cu(3)−Cl(1)#6	92.02(13)
O(4)−Cu(1)−O(6)#2	97.98(16)	O(2)#2-Cu(3)−Cl(1)#6	98.89(13)
O(5)−Cu(1)−O(6)#2	117.14(16)	Cl(1)−Cu(3)−Cl(1)#6	88.94(6)
O(5)#3-Cu(2)−O(5)#4	180.00(4)	O(4)−Cu(2)−O(3)#5	106.81(16)
O(5)#3-Cu(2)−O(4)	90.66(17)	O(4)#5-Cu(2)−O(3)#5	73.19(16)
O(5)#4-Cu(2)−O(4)	89.34(17)	O(5)#3-Cu(2)−O(3)	87.47(16)
O(5)#3-Cu(2)−O(4)#5	89.34(17)	O(5)#4-Cu(2)−O(3)	92.53(16)
O(5)#4-Cu(2)−O(4)#5	90.66(17)	O(4)−Cu(2)−O(3)	73.19(16)
O(4)−Cu(2)−O(4)#5	180.000(1)	O(4)#5-Cu(2)−O(3)	106.81(16)
O(5)#3-Cu(2)−O(3)#5	92.53(16)	O(3)#5-Cu(2)−O(3)	180.0
O(5)#4-Cu(2)−O(3)#5	87.47(16)		

[a] Note symmetry transformations used to generate equivalent atoms: #1 $x, -y+3/2, z-1/2$; #2 $-x+1, -y+1, -z$; #3 $x, -y+3/2, z+1/2$; #4 $-x+1, y-1/2, -z+1/2$; #5 $-x+1, -y+1, -z+1$; #6 $-x, -y+1, -z$.

(Quantum Design, San Diego, CA) in the temperature range 1.8 K ≤ T ≤ 250 K on a sample of ∼1.1 mg of randomly oriented crystallite polycrystalline sample. The addenda heat capacities of a minute amount of Apiezon N grease used to thermally couple the sample to the platform and the heat capacity of the platform were determined in a separate run and subtracted.

Raman scattering experiments were performed in quasi backscattering geometry using a λ = 532 nm laser line with a power of P = 2 mW. A single crystalline sample was installed into a He-cooled closed cycle cryostat with a temperature range of 3.5−300 K.

The spectra were collected via a Dilor-XY-500 triple spectrometer by a liquid nitrogen cooled HORIBA Jobin Yvon CCD (Spectrum One CCD-3000 V).

Results and Discussion

Crystal Structure. The new copper selenite chloride $Cu_5(SeO_3)_4Cl_2$ crystallizes in the monoclinic space group $P2_1/c$. The unit cell is a = 10.9104(8) Å, b = 8.3134(6) Å, c = 7.5490(5) Å, and β = 90.71(1)°. EDS analysis on some selected single crystals confirmed the stoichiometry of atoms heavier than oxygen and gave a mean composition of 45.9 at% Cu, 34.7 at% Se, and 19.5 at% Cl in good agreement with results from the refinement of the single crystal diffraction data: 45.5 at% Cu, 36.4 at% Se, and 18.2 at% Cl. Bond valence sum (BVS) calculations according to Brown and Altermatt[30] support that the Se and Cu ions have the charge +4 and +2, respectively; see Supporting Information.

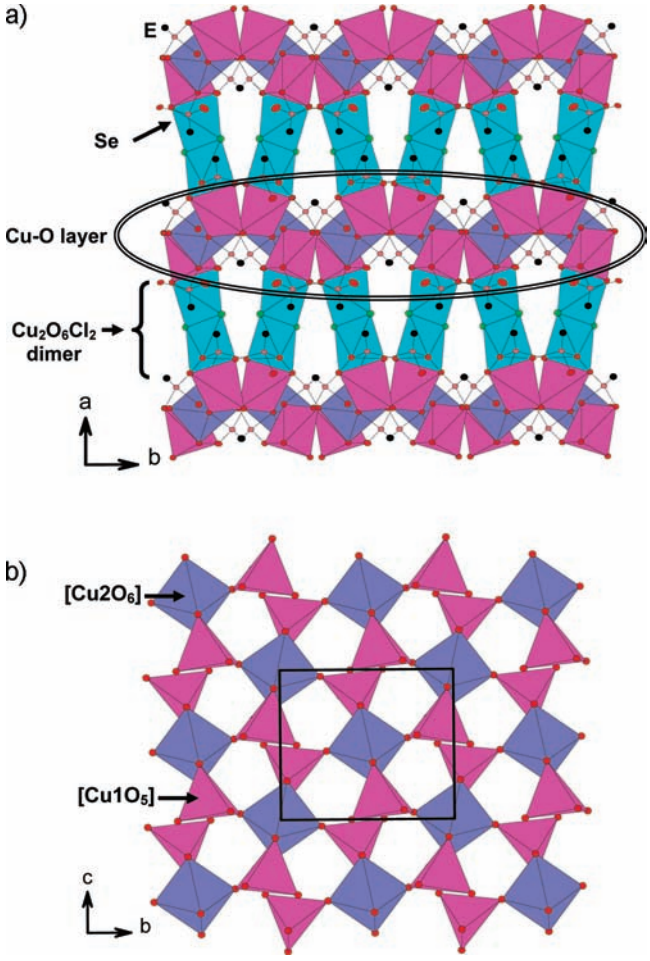

Figure 1. (a) Polyhedron view of the $Cu_5(SeO_3)_4Cl_2$ crystal structure along [001]. The pink [$Cu1O_5$] and dark blue [$Cu2O_6$] polyhedra together form Cu−O slabs that are connected by light blue [$Cu3O_3Cl_2$] polyhedra. O atoms are red; Cl atoms are green; Se atoms are orange. (b) A copper oxide slab along [100].

The crystal structure can be described as a three-dimensional framework of corner and edge sharing Cu-coordination polyhedra. There are three crystallographically different Cu atoms having distorted coordination polyhedra. Cu1 has a 5-fold [$Cu1O_5$] distorted square pyramid, where atoms O2, O3, O4, and O5 form the basal square plane with Cu−O bond distances ranging between 1.907(4) Å to 2.045 Å and O6 at the apex with a longer bonding distance 2.333(4) Å. Cu2 bonds to six oxygen atoms to form [$Cu2O_6$] Jahn−Teller distorted octahedra. The two longer Cu−O bond distances are 2.374(5) Å, and the other four bonds are in the range 1.969(4)−1.998(5) Å. Cu3 is surrounded by three oxygen and two chlorine atoms to form a [$Cu3O_3Cl_2$] distorted square pyramid; O1, O6, Cl1, and Cl1 occupy the plane positions, and the O2 atom is located at the apex.

The [$Cu2O_6$] polyhedra connect to four [$Cu1O_5$]: to two by corner sharing and to two by edge sharing, resulting in a copper oxide slab parallel to (011). The [$Cu1O_5$] polyhedra further connect to a [$Cu3O_3Cl_2$] by an O2···O6 edge completing a layer. The layers are connected by two [$Cu3O_3Cl_2$] units that have a common edge Cl1···Cl1, to form [$Cu_2O_6Cl_2$] dimers that bridge the layers to build up

(30) Brown, I. D.; Altermatt, D. *Acta Crystallogr.* **1985**, *B41*, 244–247.

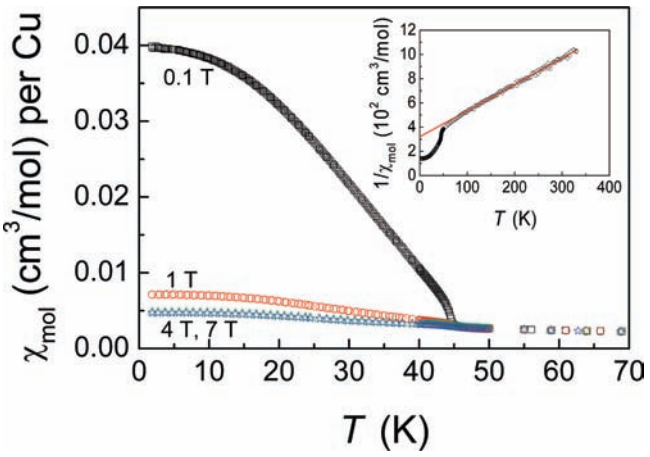

Figure 2. Magnetization (per Cu atom) measured by cooling the sample in fields of 0.1, 1, and 4 T as indicated. The inset displays the inverse magnetic susceptibility per Cu atom. The (red) solid line represents an extended Curie−Weiss law according to eq 1 with fitted parameters: $\chi_0 = +19(2) \times 10^{-6}$ cm^3/mol, $g = 2.25$, and $\theta = -151(4)$ K.

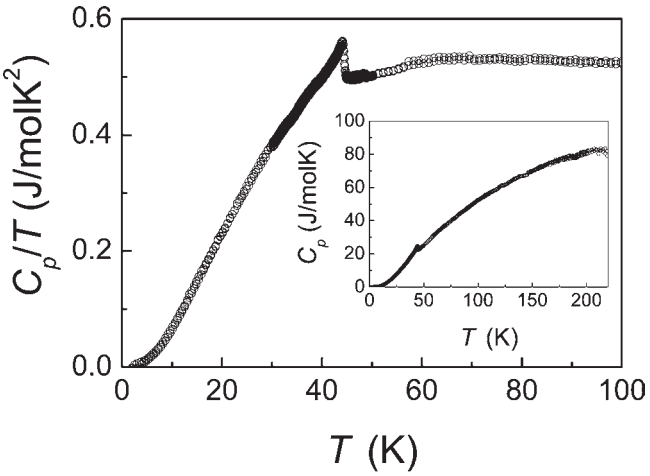

Figure 3. Heat capacity of $Cu_5(SeO_3)_4Cl_2$ (per formula unit $Cu(SeO_3)_{0.8}Cl_{0.4}$). The inset shows C_p/T vs T. The entropy contained in the anomaly at 44.1(0.2) K amounts to about 0.5(1) J/mol·K or 9(2) % of the entropy expected for a $S = 1/2$ system.

the three-dimensional framework; see Figure 1a,b. The two crystallographically different Se atoms both have a one-sided 3-fold coordination [SeO_3E]. (E is the $4s^2$ lone pair on the selenium atom.) The [SeO_3E] groups connect by corner and edge sharing to the copper oxohalide framework. However, the [SeO_3E] polyhedra are isolated from each other, in analogy with earlier observations that such polyhedra do not polymerize.[31]

Magnetic Properties. Figures 2 and 3 display the magnetic susceptibility and heat capacity data of $Cu_5(SeO_3)_4Cl_2$. Field-cooled magnetization measurements in low fields (0.1 T) reveal spontaneous polarization below a critical temperature of $T_c \sim 45$ K with an almost linear increase of the magnetization below T_c and a saturation at low temperatures. The spontaneous magnetization is readily suppressed by increasing the magnetic field. At fields above ~4 T, saturation occurs and the susceptibility becomes independent of the applied magnetic field.

Above T_c, the inverse magnetic susceptibility grows almost linear with increasing temperature with a slight negative curvature immediately above T_c. Above 150−200 K, the inverse susceptibility follows an extended Curie−Weiss law behavior according to (1)

$$\chi_{mol} = \frac{C}{(T-\Theta)} + \chi_0 \quad (1)$$

with the Curie−Weiss temperature Θ and the Curie constant C. The temperature independent term, $\chi_0 = \chi_{dia} + \chi_{vv}$, accounts for the diamagnetic susceptibility of the closed electron shells of all constituents and for temperature independent paramagnetic Van Vleck contributions of the Cu^{2+} ion. The diamagnetic susceptibility of the electrons in closed shells can be estimated by summing the increments of the ions as tabulated, e.g., by Selwood[32] (Cu^{2+}: -11×10^{-6} cm^3/mol; SeO_3^{2-}: -44×10^{-6} cm^3/mol; Cl^-: -26×10^{-6} cm^3/mol). This results in a total diamagnetic contribution of $\chi_{dia} = -283 \times 10^{-6}$ cm^3/mol per formula unit. The paramagnetic Van Vleck contributions per Cu^{2+} cation are of the order of $\sim+50 \times 10^{-6}$ cm^3/mol.[33,34]

The Curie constant is related to the effective magnetic moment, $\mu_{eff}/\mu_B = g[S(S+1)]^{1/2}$ of the Cu^{2+} cations according to (2).

$$C = \frac{N_A}{V}\frac{{\mu_{eff}}^2}{3k_B} \quad (2)$$

For Cu^{2+} with a $3d^9$ configuration and one hole in the $3d$ shell ($S = 1/2$), one expects g-factors between ~2.05 and ~2.25, enhanced over the free-electron g-factor due to spin−orbit coupling effects, depending on the direction of the applied magnetic field.[33] When fitting the experimental data for temperatures above ~150 K with $\chi_0 = \chi_{dia} + \chi_{vv} \approx -35 \times 10^{-6}$ cm^3/mol (per Cu atom) as estimated above, we arrived at negative Curie−Weiss temperatures of −151(4) K, indicating predominant antiferromagnetic spin-exchange interaction, and at an effective moment of the order of 2.19 μ_B corresponding to a g-factor of 2.25(2).

The heat capacity shows a λ-type anomaly at 44.1(2) K indicating long-range ordering in good agreement with the magnetic susceptibility measurements. The entropy removed in the magnetic ordering amounts to only about 9(2)% of the total entropy expected for a $S = 1/2$ system, implying that the essential fraction of the entropy must be removed in short-range ordering processes above the Néel temperature. However, the typical broad maximum in the magnetic susceptibility due to such correlations is not visible. The negative Curie−Weiss temperature implies predominant antiferromagnetic spin exchange interaction. On the other hand, a closer inspection of the interconnectivity of the magnetic Cu cations via the anions, Cl and O (see Figure 4), reveals that the Cu(1) and Cu(2) atoms connect via O anions with bonding angles typically in excess of 90°, leading to antiferromagnetic superexchange interaction. The Cu(1)−Cu(2) oxygen

(31) Mao, J.-G.; Jiang, H.-L.; Kong, F. *Inorg. Chem.* **2008**, *47*, 8498–8510.
(32) Selwood, P. W. *Magnetochemistry*, 2nd ed.; Interscience: New York, 1956.
(33) Lueken, H., *Magnetochemie*; Teubner Verlag, Stuttgart, and Leipzig, 1999.
(34) Banks, M. G.; Kremer, R. K.; Hoch, C.; Simon, A.; Ouladdiaf, B.; Broto, J.-M.; Rakoto, H.; Lee, C.; Whangbo, M.-H. *Phys. Rev.* **2009**, *B80*, 024404.

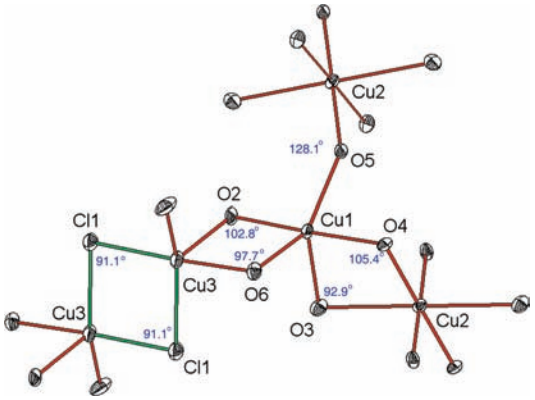

Figure 4. Connection of the different Cu-polyhedra [Cu1O_5], [Cu2O_6], and [Cu3O_3Cl_2]. The Cu−O−Cu angles are >90° while the Cu−Cl−Cu angles are ~90°; see text for discussion on how the magnetic properties may correlate with the superexchange angles.

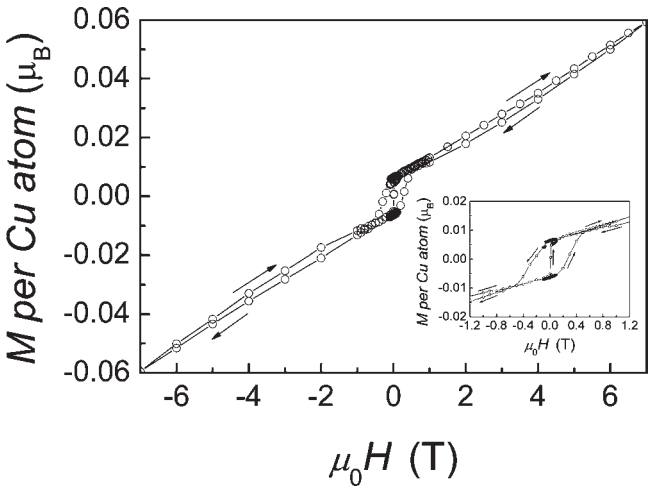

Figure 5. Hysteresis loop measured at 1.87 K. The arrows indicate the direction of field change.

slabs interact via Cu(3)−Cl bidentate bonds with Cu−Cl−Cu bonding angles of ~91°. Such bonding angles typically support ferromagnetic spin-exchange interaction and, thus, could be the origin of the ferromagnetic contributions in the overall spin exchange.[35]

Field dependent magnetization measurements at 1.87 K show a hysteresis of the magnetization with a typical hysteresis loop of a ferromagnetic material; see Figure 5. The symmetric hysteresis loop closes above/below fields of 0.5T/−0.5T, respectively. Above these field values, the magnetizations are linear and largely independent of the history. The hysteresis points to weak ferromagnetic behavior with a saturation moment of ~0.01 μ_B, with a canting angle of less than a degree, assuming an ordered moment of 1 μ_B per Cu atom.

Raman Scattering. In Figure 6, we give an overview of the Raman spectra taken at different discrete temperatures ranging from 3 to 295 K. The spectra were collected on platelike single crystals in $x(yy)x$ polarization, i.e., in parallel light polarization with x and y both within the ab plane. The displayed regime covers the frequencies from

(35) Bencini, A.,; Gatteschi, D. *EPR of Exchange Coupled Systems*; Springer Verlag: Berlin, Heidelberg, 1990.

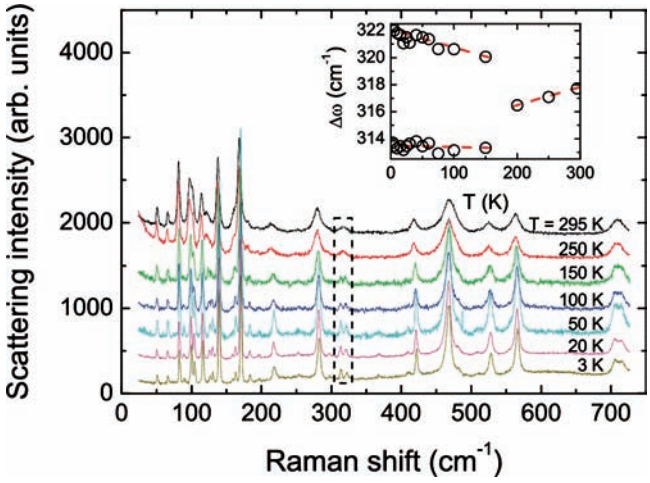

Figure 6. Raman spectra of $Cu_5(SeO_3)_4Cl_2$ obtained in the temperature range 3−295 K in parallel polarization. The inset gives the frequency shift of the mode at 317 cm^{-1} that splits with decreasing temperature.

25 to 725 cm^{-1}. Four further phonon modes are observed at higher energies (742, 802, 848, and 854 cm^{-1}). They will be neglected in the following, as they do not show any anomalies in the temperature range covered.

$Cu_5(SeO_3)_4Cl_2$ crystallizes in the monoclinic space group $P2_1/c$. Symmetry analysis yields a total of $\Gamma_{Raman} = 33*A_g + 33*B_g$ Raman active modes, with

$$A_g = \begin{pmatrix} a & d & 0 \\ d & b & 0 \\ 0 & 0 & c \end{pmatrix} \quad \text{and} \quad B_g = \begin{pmatrix} 0 & 0 & e \\ 0 & 0 & f \\ e & f & 0 \end{pmatrix}$$

In our spectra, we observe 33 phonon modes in good agreement with the above analysis. These modes are attributed to A_g symmetry. Despite several checks, we could not resolve the B_g modes, which we attribute to the platelike sample geometry. In the temperature range 200−100 K, several A_g modes exhibit a splitting with decreasing temperature (observed at 125, 317, and 710 cm^{-1}). The inset of Figure 6 gives, as an example, the temperature dependence of the mode at 317 cm^{-1}. This effect may indicate structural distortions or a pronounced anharmonicity, which could be related to a coupling to the spin system. In order to search for a structural transformation, we performed low temperature single crystal XRD measurements at T = 100 K. However, crystallographic changes from the room temperature structure were not detected, indicating that the ordering induced lattice deformation might be of minor magnitude. Because of the small sample mass, our heat capacity data are increasingly noisy above ~100 K, limiting a conclusive statement from this technique. Nevertheless, no indication of a structural phase transition between 150 and 200 K has been observed.

The polyhedra [Cu2O_6] and their connections to [Cu1O_5] are rather distorted and do not contain inversion centers (see Figure 4). From general symmetry grounds, antisymmetric Dzyaloshinskii-Moriya (DM) spin exchange is, therefore, allowed which leads to weak ferromagnetic moments in applied magnetic fields as observed in the magnetization measurements. As the strength of this interaction is intimately related to the Cu−O bond length

and angles, it also enhances spin−phonon interactions. As an example, we refer to the chain system $KCuF_3$[36] where ESR evidence coupled spin−lattice fluctuations and phonon modes show related shoulders and weak splittings in Raman scattering experiments.[37] In this respect, $Cu_5(SeO_3)_4Cl_2$ shares some similarities with $KCuF_3$, as both weak ferromagnetic moments and weak lattice distortions coexist. Further experimental studies beyond the scope of the present investigation are needed to substantiate this interpretation. It is noted that the occurrence of antisymmetric DM spin exchange and the related spin phonon interaction may also induce a coupling of dielectric and magnetic properties in the form of magnetocapacitance, a larger dependence of the dielectric constant on the magnetic field, or even multiferrocity with coexisting spontaneous ferroelectric and ferromagnetic moments. As an example, we mention the structurally closely related system $FeTe_2O_5Br$[17] that shows multiferroic behavior.[18] $Cu_5(SeO_3)_4Cl_2$ may similarly be a candidate for such a coupling of ferroelectric and magnetic order parameters.

Summary and Conclusions

The new copper selenite chloride $Cu_5(SeO_3)_4Cl_2$ crystallizes in the monoclinic space group $P2_1/c$. The crystal structure can be described as a three-dimensional framework of corner and edge sharing Cu-coordination polyhedra: $[CuO_5]$, $[CuO_6]$, and $[CuO_3Cl_2]$. The Se atoms have a one-sided 3-fold coordination $[SeO_3]$ that connect to the Cu-polyhedra by corner and edge sharing but are isolated from each other in analogy with earlier observations that such polyhedra do not polymerize. The coordination polyhedra arrange so that oxide layers are formed that extend parallel to the (100) plane. The oxide layers are bridged to build up the three-dimensional framework by that $[CuO_3Cl_2]$ unit from different layers having a common Cl···Cl edge.

Most compounds described in the Cu^{2+}−Se^{4+}−O−Cl system are three-dimensional framework systems like the present one where the framework is made up of corner and edge sharing Cu-polyhedra and the $[SeO_3]$ polyhedra do not polymerize.[2,21−25,27] The only phase that is layered with only weak Van der Waal interactions in between the layers is β-$Cu_3(SeO_3)_2Cl$.[26] For corresponding compounds with Te^{4+}, it is much more common with layered structures with weak interactions in between the layers and rarer with three-dimensional framework structures.

Field-cooled magnetization measurements in low-fields (0.1 T) reveal a spontaneous polarization below a critical temperature of $T_c \sim 45$ K with an almost linear increase of the magnetization below T_c and saturation at low temperatures. In good agreement with this indication for long-range order, the heat capacity shows a λ-type anomaly at 44.1(2) K. An analysis of the high temperature magnetic susceptibility leads to a negative Curie−Weiss temperature of −151(4) K, indicating predominant antiferromagnetic spin-exchange interaction and at an effective moment of the order of 2.19 μ_B, corresponding to a g-factor of 2.25(2). The reduction of the ordering temperature compared with the mean exchange interaction is attributed to the reduced connectivity and distorted exchange paths.

Field dependent magnetization measurements at 1.87 K reveal a slight hysteresis with a hysteresis loop which closes above/below fields of 0.5T/−0.5 T, respectively. The hysteresis is ascribed to weak ferromagnetic behavior with a saturation moment of ~0.01 μ_B and a canting of the Cu moments with a canting angle of less than a degree. We attribute this canting to Dzyaloshinskii−Moriya (DM) spin exchange based on distorted $[Cu2O_6]$ polyhedra and their connections to $[Cu1O_5]$ that do not contain inversion centers. The evidence for structural distortions seen as a splitting of several phonon modes in Raman scattering in the temperature range 100−200 K could also be related to DM interaction. However, we found no evidence for significant crystallographic changes in low temperature single crystal XRD measurements. Concluding, new copper selenite chloride $Cu_5(SeO_3)_4Cl_2$ is both from structural chemistry as well as from a physics point of view an interesting compound and well comparable to earlier found lone pair oxohalides.

Acknowledgment. This work has been carried out in part through financial support from the Swedish Research Council and the German Science Foundation (DFG). We thank E. Brücher and G. Siegle for expert experimental assistance.

Supporting Information Available: Experimental and simulated powder X-ray diffraction patterns and results from bond valence sum (BVS) calculations. This material is available free of charge via the Internet at http://pubs.acs.org. Further details on the crystal structural investigations of this compound may be obtained from the Fachinformationszentrum Karlsruhe, Abt. PROKA, 76344 Eggenstein-Leopoldshafen, Germany (Fax +49-7247-808-666; E-mail: crysdata@fiz-karlsruhe.de), on quoting the depository numbers CSD-380282.

(36) Eremin, M. V.; Zakharov, D. V.; Krug von Nidda, H.-A.; Eremina, R. M.; Shuvaev, A.; Pimenov, A.; Ghigna, P.; Deisenhofer, J.; Loidl, A. *Phys. Rev. Lett.* **2008**, *101*, 147601.

(37) Gnezdilov, V.; Deisenhofer, J.; Lemmens, P.; Wulferding, D.; Afanasiev, O.; Ghigna, P.; Loidl, A.; Yeremenko, A. arXiv:1003.1666, **2010**. Prepublication database from Cornell University Library.